

Microstructure and a Nucleation Mechanism for Nanoprecipitates in PbTe-AgSbTe₂

Xuezhi Ke,^{1,2,*} Changfeng Chen,^{1,†} Jihui Yang,^{3,‡} Lijun Wu,⁴ Juan Zhou,⁴ Qiang Li,⁴ Yimei Zhu,^{4,§} and P. R. C. Kent⁵

¹*Department of Physics and High Pressure Science and Engineering Center, University of Nevada, Las Vegas, Nevada 89154, USA*

²*Department of Physics and Institute of Theoretical Physics, East China Normal University, Shanghai 200062, China*

³*Materials and Processes Laboratory, General Motors R&D Center, Warren, Michigan 48090, USA*

⁴*Condensed Matter Physics and Materials Science Department, Brookhaven National Laboratory, Upton, New York 11973, USA*

⁵*Center for Nanophase Materials Sciences, Oak Ridge National Laboratory, Oak Ridge, Tennessee 37831, USA*

(Received 1 October 2008; published 2 October 2009)

Many recent advances in thermoelectric (TE) materials are attributed to their nanoscale constituents. Determination of the nanocomposite structures has represented a major experimental and computational challenge and eluded previous attempts. Here we present the first atomically resolved structures of high performance TE material PbTe-AgSbTe₂ by transmission electron microscopy imaging and density functional theory calculations. The results establish an accurate structural characterization for PbTe-AgSbTe₂ and identify the interplay of electric dipolar interactions and strain fields as the driving mechanism for nanoprecipitate nucleation and aggregation.

DOI: 10.1103/PhysRevLett.103.145502

PACS numbers: 61.46.-w, 62.23.Pq, 71.15.Nc, 72.15.Jf

Advanced thermoelectric (TE) materials attract considerable current interest [1–12]. A particularly interesting case is the (PbTe)_{1-x}(AgSbTe₂)_x ($x \sim 0.05$) nanocomposites that exhibit very high TE efficiency measured by the figure of merit parameter $ZT \sim 2.1$ at 800 K [6,12]. It has been recently recognized that the presence of nanoprecipitates is likely key to producing high ZT values. A prerequisite to understanding TE properties is an accurate determination of the microstructure of these complex nanocomposites, especially the atomic arrangement and nucleation mechanism, which presents a grand challenge [13]. On the experimental side, x-ray and neutron diffraction usually leave some degree of ambiguity in atomic position assignment since coexisting phases in nanocomposites hinder structural refinement. High resolution transmission electron microscopy (HRTEM) is well suited to study local structural inhomogeneity, but a quantitative analysis is often difficult without adequate theoretical support, which has plagued recent attempts [6,12]. On the computational side, a nanocomposite containing a minority phase at low doping necessitates the use of very large supercells that pushes the limit of current computing capability. Despite extensive past work, there remains considerable controversy and uncertainty on the atomic arrangement and nucleation mechanism of AgSbTe₂ in PbTe [12,14,15]. Recent theoretical efforts on the atomic ordering in AgSbTe₂ nanoclusters [16,17] provide interesting insights into the structural features of AgSbTe₂, but they were unable to adequately account for the effect of stress release at the interface of the nanoclusters and the PbTe matrix, which plays a pivotal role in determining the stable structure.

In this Letter we report a combined experimental and computational effort that establishes the first unambiguous atomically resolved structural assignment for the

(PbTe)_{1-x}(AgSbTe₂)_x nanocomposite and identifies the mechanisms for the nucleation and atomic arrangement of the nanoprecipitates. The atomistic features were probed using a double aberration corrected HRTEM instrument with a subangstrom spatial resolution [18,19] on single crystal (PbTe)₁₈-(AgSbTe₂)₁ grown by the Bridgeman technique. The density functional theory (DFT) calculations employed a massive 39.3 Å × 39.3 Å × 39.3 Å supercell containing 1728 atoms which can accommodate the composite system with the size of the fully enclosed nanoprecipitate reaching those observed in actual specimens [20]. It allows for the first time a close examination of the nucleation of the nanoprecipitates in the host matrix with fully atomistically relaxed structures at high accuracy.

Figure 1 shows HRTEM images of (PbTe)₁₈-(AgSbTe₂)₁ and the structures obtained from DFT calculations. Two nanoprecipitate shapes are most commonly seen throughout the entire sample. One is platelike and the other is cubelike, as shown in Fig. 1(a), both with diffused contrast. Our HRTEM study also observed some Pb-rich regions in the sample, which is consistent with recent X-ray PDF work that reveals that the nanoprecipitates contain substantial Pb [21]. A careful analysis of our results indicates that these regions are composites consisting of several smaller nanoprecipitates in the PbTe matrix. The plate- and cubelike nanoprecipitates identified by our HRTEM data and fully supported by our DFT calculations represent the energetically most favorable nanoclusters of the AgSbTe₂ phase in PbTe. A striking feature unraveled by our calculations is the extraordinary large atomic deviations from the ideal atomic positions in the nanoprecipitates, particularly at the Ag sites (up to 2.35 Å or 72% of an ideal bond length). This finding is made possible by the use of our large supercell and is corroborated by the HRTEM measure-

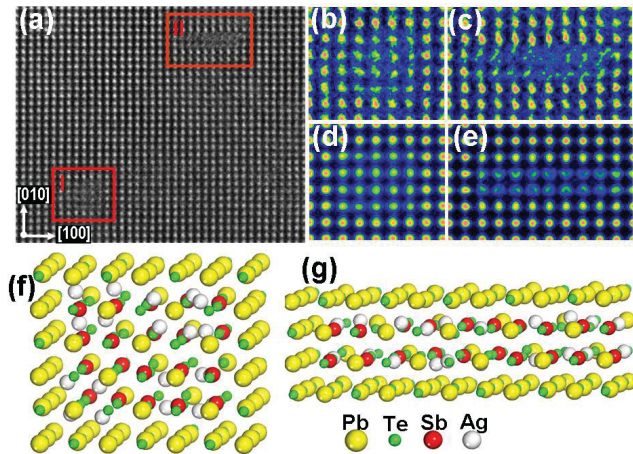


FIG. 1 (color). (a) HRTEM image of a single crystal $(\text{AgSbTe}_2)\text{-(PbTe)}_{18}$ sample. The red squares I and II highlight two typical nanoprecipitates in the sample. (b) and (c) are the magnified images of I and II, respectively, and the corresponding simulated images in (d) and (e) are based on the atomic positions predicted by our DFT calculations shown in (f) and (g), respectively. The diffusive nature of the nanoprecipitates is caused by Ag atoms taking interstitial positions. Panel (a) also demonstrates the $\langle 100 \rangle$ preferential growth direction in full agreement with the DFT calculations.

ment. Figures 1(d) and 1(e) show the HRTEM simulated images based on the multislice calculations using electron dynamic scattering theory [22] with DFT calculated atomic positions [Fig. 1(f) and 1(g)] as input. The simulated images are in excellent agreement with the experimental observations [Fig. 1(b) and 1(c)]. The observed contrast delocalization of the nanoprecipitates is due to the large atomic displacement of Ag atoms from their ideal positions. To characterize the disorder of this system, the radial distribution function was calculated [20], and the result is comparable to the experimental data [21]. Our calculations also reveal additional features crucial to understanding this novel nanocomposite material: (i) the Ag-Te-Sb-Te (Ag-Sb for short) pairs, which are the smallest building blocks of the (AgSbTe_2) minority phase, show preferential growth along the $\langle 001 \rangle$ directions in PbTe matrix, and (ii) these pairs tend to form four-pair clusters which, in turn, become the building blocks for larger nanoprecipitates. These atomistic structural features are verified by our HRTEM measurements [Fig. 1(a)]. The observed thin-plate-shaped nanoprecipitates of 2 to 3 nanometers in size are in excellent agreement with our DFT calculations (see below). Our calculations reveal that a large supercell is extremely important for accurate determination of the atomic arrangement for AgSbTe_2 nanoprecipitates in PbTe matrix. This is illustrated in Fig. 2 where two $\text{Ag}_{20}\text{Sb}_{20}$ nano-clusters with the same size and growth direction but subtle differences in atomic ordering and dipole coupling patterns are examined. When a small unit cell is used, we found that

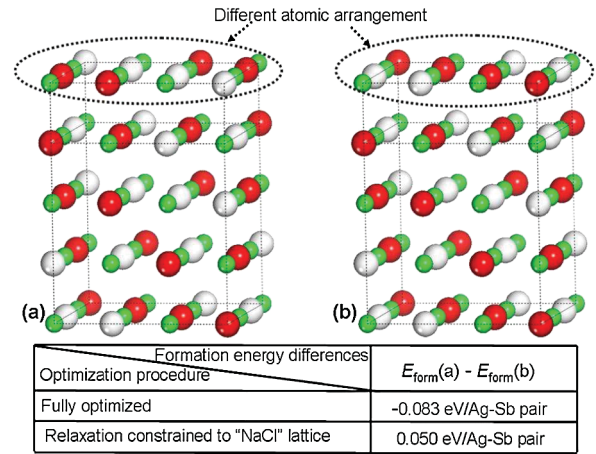


FIG. 2 (color). Top panel: Two structures (a) and (b) of nano-cluster $\text{Ag}_{20}\text{Sb}_{20}$ in the $\text{Ag}_{20}\text{Pb}_{824}\text{Sb}_{20}\text{Te}_{864}$ supercell. Bottom panel: Their formation energy difference obtained using constrained or full structural relaxation.

the lattice stress cannot be released, and thus the displacement of doped Ag atoms cannot be observed, which leads to a NaCl lattice for the doped atoms. If the doped atoms are constrained to the NaCl lattice, Fig. 2 shows that structure (a) is energetically less favorable than (b) by 0.050 eV/Ag-Sb pair. When this constrain is released, however, structure (a) becomes more stable by 0.083 eV/Ag-Sb pair. This qualitative reversal of relative stability with a fairly large energy difference stems from proper release by full structural relaxation of large residual stresses in the small supercell (see below for more details). It underscores the pivotal role of full stress release in the structural determination and suggests that recent calculations using free-standing or lattice-constrained AgSbTe_2 cells [16,17] are inadequate in determining the most energetically favorable atomic ordering in the nanoprecipitates.

We now explore the atomistic growth mechanism for AgSbTe_2 nanoprecipitates in PbTe. The first key issue on Ag/Sb doping in bulk PbTe is how an individual Ag-Sb pair arranges in the PbTe lattice. Previous studies [14,15] were inconclusive on this issue because their use of smaller supercells with periodic boundary conditions introduce unrealistic configurations (e.g., the infinite -Ag-Te-Sb-Te-chain in the $\langle 100 \rangle$ direction in the 64-atom supercell) and cause large finite-size errors. This problem is adequately addressed in our calculations where the use of the much larger 1728-atom supercell allows an accurate determination of the energy of incipient Ag-Sb pair. Figure 3 shows the calculated formation energies for a Ag-Sb pair in PbTe along various directions in the (001) plane. The nearest-neighbor (NN) Ag-Te-Sb pairing along the $\langle 100 \rangle$ direction is the energetically preferred arrangement, in agreement with the HRTEM results [Fig. 1(a)]. We also examined pairs aligned out of the (001) plane (e.g., along the [111], [211], and [241] directions) and found that they all have higher (above 0.08 eV/pair) energies.

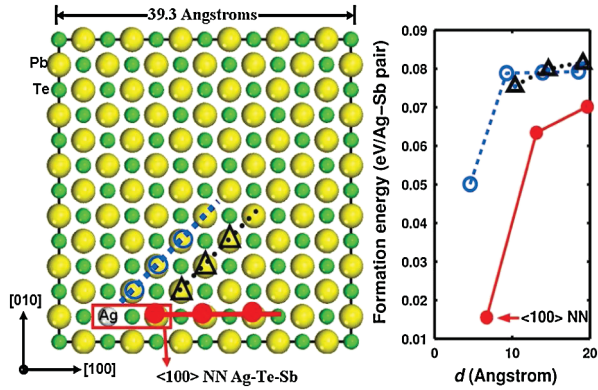


FIG. 3 (color). Arrangements of a Ag-Sb pair in PbTe matrix in the (001) plane of the 1728-atom ($12 \times 12 \times 12$ atoms) supercell (left) and their formation energies versus Ag-Sb distance d indicated by the same symbols (right).

We next examine the arrangement of two Ag-Sb pairs in PbTe, which offers key insights for the incipient nucleation mechanism of the minority AgSbTe_2 phase. Six representative arrangements in the (001) plane of the $\text{Ag}_2\text{Pb}_{860}\text{Sb}_2\text{Te}_{864}$ supercell and their energies are displayed in Fig. 4 [typical out-of-plane arrangements were checked and found to have higher energies than arrangement (a)]. The square arrangement (a) with a maximal number of Ag-Sb pairings has the lowest energy, which can be understood by an electric dipole model, considering that the $\text{Ag}(+1)$ and $\text{Sb}(+3)$ substitutions cause charge depletion and enhancement relative to the original $\text{Pb}(+2)$ sites. The maximally paired configuration shown in Fig. 4(a) is the expected lowest-energy state for a two-dipole system. This dipolar interaction model also proves useful for interpreting more complex structural features of the nanoprecipitates obtained in the DFT calculations and HRTEM measurements presented below. Based on the above results we can summarize two basic rules for Ag and Sb doping in PbTe: (i) Ag and Sb prefer to form NN

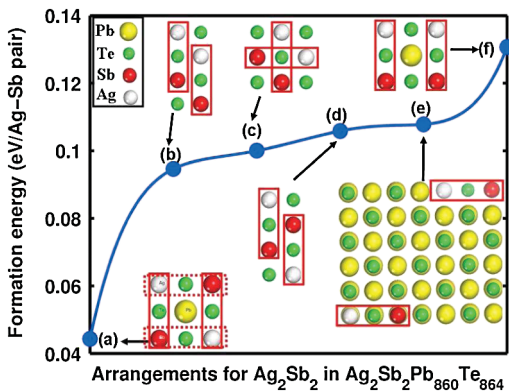


FIG. 4 (color). Calculated formation energy for various arrangements of two Ag-Sb pairs in $\text{Ag}_2\text{Sb}_2\text{Pb}_{860}\text{Te}_{864}$ (the supercell is partially shown). Each Ag-Sb pair is marked by a red rectangle as a guide for the eye.

pairs along the $\langle 100 \rangle$ direction of the PbTe matrix, behaving like electric dipoles in structural and energetic characteristics, and (ii) the Ag-Sb pairs tend to form a maximal number of Ag-Sb pairings. However, as shown below, lattice strain imposes additional constraints on this dipolar scheme.

We performed extensive calculations for a series of $\text{Ag}_n\text{Pb}_{864-2n}\text{Sb}_n\text{Te}_{864}$ and examined a large number of atomic arrangements in each case [20]. Figure 5 shows the most stable arrangements and their energies for nanoprecipitates up to $n = 40$. The formation of AgSbTe_2 nanoprecipitates is clearly preferred over a uniform dispersion of Ag and Sb atoms in PbTe. For $n \leq 16$, the atomic

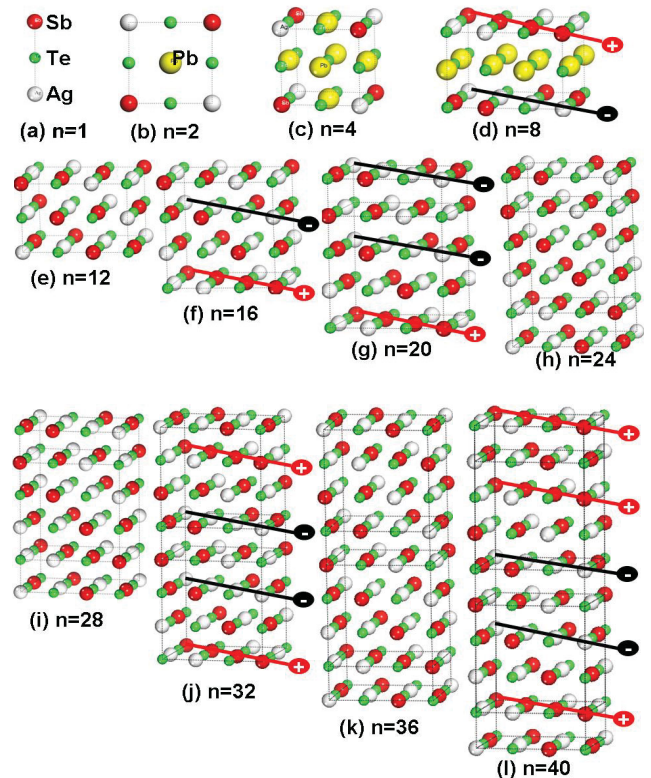


FIG. 5 (color). Top panel: The atomic orderings for the most stable nanoclusters Ag_nSb_n in $\text{Ag}_n\text{Pb}_{864-2n}\text{Sb}_n\text{Te}_{864}$ with $n = 1, 2, 4, 8, 12, 16, 20, 24, 28, 32, 36,$ and 40 [(a) to (l)]. The thick lines and $+/-$ signs indicate the arrangements of dipoles formed by $\text{Ag}(-)$ and $\text{Sb}(+)$ atoms. Other notations are the same as in Fig. 4. Bottom panel: The calculated formation energies (in eV/Ag-Sb pair).

orderings follow the electric dipole rule, namely, the dopant atoms prefer to form a maximal number of Ag-Sb pairing. The formation energy undergoes a sharp decrease at $n = 4$ and again at $n = 16$, both consistent with the dipole model, and then stays at near constant values for larger n . A close analysis reveals that for $n > 16$, additional dopant atoms tend to break the Ag-Sb pairing pattern along the column growth direction; instead, the Ag-Te-Ag (Sb-Te-Sb) pairing, still aligned along the $\langle 100 \rangle$ directions, becomes more favorable. This phenomenon can be attributed to the interplay between the dipole interactions and lattice strain: Initially, the Ag-Te-Sb pairs (dipoles) tend to form plate or column structures with Ag matched against Sb sites to maximize the energetic gain. Meanwhile, such nanoclusters induce local strain due to their lattice mismatch with the PbTe host matrix that tends to break the dipole pairing pattern. Consequently, the breaking of the normal dipole arrangement gives rise to the lowest-energy configuration, reflecting the balance between the dipole-dipole attraction and the strain relaxation at the cluster-host matrix boundary. These results suggest that the aggregation of the AgSbTe₂ minority phase in PbTe would likely produce nanoprecipitates containing 16 or 20 Ag-Sb pairs arranged in column or plate shapes since further Ag-Sb aggregation would have minimal additional energy gain and would likely be impeded by kinetic barriers. Significant Ag atomic position deviation is observed inside these nanoprecipitates. These are all in agreement with our HRTEM experiments. The overall size and morphology variations of the composite nanoprecipitates observed in experiments are likely governed by a Boltzmann distribution among energetically comparable states and growth kinetics. Consequently, nanoprecipitates with other shapes and larger composites containing several closely packed nanoprecipitates are also observed in our HRTEM (not shown here) and previous experiments [6,12,21].

To conclude, our combined DFT calculations and HRTEM measurements resolve the nanostructural features and provide a realistic full-scale view of the AgSbTe₂ nanoprecipitate nucleation and interaction in PbTe. The nucleation is driven by the intrinsic interplay between the electric dipolar attraction and strain energy release. Significant deviations of atomic positions away from the ideal lattice sites inside the nanoprecipitates are revealed by the calculations and corroborated by the HRTEM results. The calculated structural features are in full agreement with the experimentally observed nanoprecipitate orientation, size, and detailed atomic position deviation as indicated by the diffused contrast of the HRTEM images. These results shed light on a new mechanism for the formation of nanoprecipitates in complex composite materials. They represent a significant advance in enabling further explorations that require an accurate structural description. A key remaining challenge is to establish a

connection between the structural features obtained here and TE properties.

We thank Markus Eisenbach, Doug Kothe, Julia White, and D. Ray Johnson for their help with the computations. This work was supported by DOE Cooperative Agreements DE-FC52-06NA26274 (X. K., C. C.) and DE-FC26-04NT42278 (J. Y.). Work at BNL was supported by the DOE Office of Science under Contract No. DE-AC02-98CH10886. This research used resources (Cray XT4) of the National Center for Computational Sciences and the Center for Nanophase Materials Sciences at ORNL, which are sponsored by the respective facilities divisions of the DOE Offices of Advanced Scientific Computing Research and Basic Energy Sciences.

*xzke@phy.ecnu.edu.cn

†chen@physics.unlv.edu

‡jihui.yang@gm.com

§zhu@bnl.gov

- [1] Annual Energy Review 2006 (Energy Information Administration, U.S. Department of Energy, Washington, DC, 2007), <http://www.eia.doe.gov/aer>.
- [2] T. M. Tritt and M. A. Subramanian, MRS Bull. **31**, 188 (2006), and references therein.
- [3] J. Yang and T. Caillat, MRS Bull. **31**, 224 (2006), and references therein.
- [4] R. Venkatasubramanian, E. Siivola, T. Colpitts, and B. O'Quinn, Nature (London) **413**, 597 (2001).
- [5] T. C. Harman, P. J. Taylor, M. P. Walsh, and B. E. Laforge, Science **297**, 2229 (2002).
- [6] K. F. Hsu *et al.*, Science **303**, 818 (2004).
- [7] T. C. Harman *et al.*, J. Electron. Mater. **34**, L19 (2005).
- [8] H. Ohta *et al.*, Nature Mater. **6**, 129 (2007).
- [9] A. I. Hochbaum *et al.*, Nature (London) **451**, 163 (2008).
- [10] A. I. Boukia *et al.*, Nature (London) **451**, 168 (2008).
- [11] B. Poudel *et al.*, Science **320**, 634 (2008).
- [12] E. Quarez *et al.*, J. Am. Chem. Soc. **127**, 9177 (2005).
- [13] S. J. L. Billinge and I. Levin, Science **316**, 561 (2007).
- [14] D. Bilc *et al.*, Phys. Rev. Lett. **93**, 146403 (2004).
- [15] H. Hazama, U. Mizutani, and R. Asahi, Phys. Rev. B **73**, 115108 (2006).
- [16] K. Hoang, S. D. Mahanti, J. R. Salvador, and M. G. Kanatzidis, Phys. Rev. Lett. **99**, 156403 (2007).
- [17] S. V. Barabash, V. Ozolins, and C. Wolverton, Phys. Rev. Lett. **101**, 155704 (2008).
- [18] M. A. O'Keefe *et al.*, Ultramicroscopy **89**, 215 (2001).
- [19] P. D. Nellist *et al.*, Science **305**, 1741 (2004).
- [20] See EPAPS Document No. E-PRLTAO-103-039942 for experimental and computational details. For more information on EPAPS, see <http://www.aip.org/pubservs/epaps.html>.
- [21] H. Lin *et al.*, Phys. Rev. B **72**, 174113 (2005).
- [22] E. J. Kirkland, *Advanced Computing in Electron Microscopy* (Plenum, New York, 1998).